applied sciences

MDPI

Article

# Experimental Assessment of the Effect of Vertical Earthquake Motion on Underground Metro Station

**Zhiming Zhang [1,2], Emilio Bilotta [2,*], Yong Yuan [3,*], Haitao Yu [4] and Huiling Zhao [5]**

1 Department of Geotechnical Engineering, Tongji University, Shanghai 200092, China; 1410252@tongji.edu.cn
2 Department of Civil, Architectural and Environmental Engineering, University of Naples Federico II, 80125 Naples, Italy
3 State Key Laboratory of Disaster Reduction in Civil Engineering, Tongji University, Shanghai 200092, China
4 Key Laboratory of Geotechnical and Underground Engineering of Ministry of Education, Tongji University, Shanghai 200092, China; yuhaitao@tongji.edu.cn
5 Department of Civil Engineering, Shanghai University, Shanghai 200444, China; hlzhao@shu.edu.cn
* Correspondence: bilotta@unina.it (E.B.); yuany@tongji.edu.cn (Y.Y.); Tel.: +39-81-7683469 (E.B.); +86-21-65980234 (Y.Y.)

Received: 27 September 2019; Accepted: 26 November 2019; Published: 29 November 2019

check for updates

**Featured Application: This research has proven that the ratio of vertical to horizontal peak ground acceleration (RVH) has a significant influence on dynamic soil-structure interaction. It is believed that under extreme earthquake loading, such as near fault zones, RVH is a parameter of paramount importance and should be accounted for in the seismic analyses and seismic performance assessment of underground structures, especially for those with zero or near-zero buried depth, such as an atrium-style metro station. The conclusions of this research are expected to contribute to the revision of codes for seismic design of underground structures.**

**Abstract:** This paper presents experimental assessment of the effect of the ratio of vertical to horizontal peak ground acceleration (RVH) on underground metro station. An atrium-style metro station embedded in artificial soil subjected to earthquake loading is examined through shaking table tests. The experimental results for three different RVH, including soil acceleration, soil-structure acceleration difference, dynamic soil normal stress (DSNS), and structural dynamic strain, are presented and the results are compared with the case of horizontal-only excitation. It is found that for an atrium-style metro station, the differences in horizontal acceleration amplitude between the structure and the adjacent soil rise with increasing RVH, which are different at different depths. The most significant differences occur at the depth of the ceiling slab. It is also observed that both the amplitude and distribution of peak DSNS have obvious differences between the left and right side walls at all levels. It is therefore concluded that the RVH has a significant influence on dynamic soil-structure interaction. It is believed that under extreme earthquake loading, such as near fault zones, RVH is a parameter of paramount importance and should be accounted for in the seismic analyses and seismic performance assessments of underground structures, especially for those with zero or near-zero buried depth, such as atrium-style metro stations.

**Keywords:** vertical earthquake motion; seismic response; atrium-style metro station; shaking table test

## 1. Introduction

The three-dimensional behavior of underground structures during earthquakes is a matter of interest for improving the seismic analysis and design in civil engineering under extreme loads. Although extensive studies were carried out on the effects of the horizontal component of the ground shaking, only limited work has been done in the analysis of the effect of the vertical component. This topic deserves attention since some field evidence and investigations on the near-field ground motions have demonstrated that vertical components caused destructive consequences, even possible collapse, for some existing structures [1–4]. The latest developments in the underground vibration or deformation monitoring techniques such as the fiber-optic sensors [5,6] are expected to facilitate both the acquisition of the field evidence and the research work concerning the vertical earthquake motion.

In view of the fact that the ratio of vertical to horizontal peak ground acceleration (RVH) is extremely high in the vicinity of the active faults, it seems essential to study the influence of the RVH on the seismic responses of the underground structures, such as metro stations in the seismic active regions. Through numerical analyses based on the finite element-finite difference method, Uenishi and Sakurai [7] discussed the effect of the vertical oscillations and overburden on the damage-concentration mechanism of the columns at several specific underground station sections in the 1995 Hyogo-ken Nanbu (Kobe) earthquake. On the other hand, An et al. [8] discussed the effect of the vertical motion on the failure mode and dynamic response of the metro station, and concluded that in this case the vertical ground motion was not the primary cause of the collapse.

Research had also been carried out to investigate the influencing factor of RVH. Moore and Guan [9] investigated numerically the dynamic interaction of the twin tunnels subjected to the incident seismic waves. They have shown how the dynamic response of the twin tunnels depended on the incident angle of the earthquake wave, together with the spacing between two adjacent tunnels and the modulus ratio of the tunnel to the surrounding soil. Stamos and Beskos [10,11] provided insights into the dynamic responses of the underground infinitely long lined tunnels buried into an elastic or viscoelastic half-space subjected to the obliquely incident waves using the boundary element method (BEM), and proved the influence of the incident directions of the seismic waves on the dynamic responses of the tunnels. Lee and Trifunac [12] proved that the amplitudes of the stresses and deformations near the tunnel were dependent upon the angle of incidence, which determined the overall trends of the amplitudes. Lee and Manoogian [13,14] adopted the weighted residual method to study the scattering and diffraction of the plane SH-waves by an underground cavity of the arbitrary shape in a two-dimensional elastic half-space, and demonstrated same observations as for circular cavities that ground amplifications depended on the orientation of the incident waves. Wong et al. [15] studied the dynamic response of a cylindrical pipe embedded in an elastic semi-infinite medium using hybrid finite element and eigenfunction expansion techniques. They found that dynamic amplification was significantly dependent on the angle of incidence and the depth of embedment. Huang et al. [16] investigated the impact of the incident angles of earthquake shear waves (SV and SH-waves) on the seismic responses of a long lined tunnel, and numerical results indicated that non-linear seismic responses of the long lined tunnels were highly affected by the incident angles of the S-waves, which should be taken into consideration in mapping the seismic risk of the tunnels. Sun and Wang [17] investigated numerically the seismic responses of the underground rectangular tunnel under the vertical seismic excitation. Numerical results show that under vertical seismic excitation the tunnel experienced greater vertical stress from time to time and vertical compressive deformation, and sometimes it completely separated from the above soil layer.

The effect of the vertical shaking during an earthquake has been experimentally investigated previously through just a few shaking table tests. In terms of the experimental study on the tunnels, Xu et al. [18] investigated the mechanism and effect of the seismic measures of the mountain tunnel through the three-dimensional shaking table tests, where the peak ground acceleration (PGA) of the vertical input motion was taken to be 2/3 of the value corresponding to the horizontal input motion. Experimental results show that with 63% probability of exceedance in 50 years, including vertical components of the earthquakes increased the peak dynamic soil pressures on the tunnel sidewall, while the opposite was true for 1% probability of exceedance in 50 years. In both cases there was no significant change in the peak dynamic strain of the inverted arch on two sides of the flexible joints. Wang et al. [19] also adopted the above-mentioned definition of the horizontal and vertical strategies and investigated experimentally two shallow-bias tunnels with a small clear distance subjected to the horizontal–vertical earthquake excitations with different levels. Results show that the acceleration amplification factors of the vertical-direction were generally larger (1.02–3.94 times) that that of the horizontal-direction and the earthquake intensity presented different influence on the acceleration responses in the horizontal and vertical directions. In addition, Zhao et al. [20] investigated experimentally the dynamic responses of a tunnel subjected to near-fault pulse-like earthquake motions, where both vertical excitations and transverse-longitudinal-vertical excitations were included.

With respect to the underground metro stations, for example, Zhao et al. [21] studied the vibration behavior of a framed metro station under horizontal and horizontal–vertical seismic excitation using a shaking table. Experimental results show that for the lower shaking intensity the structural relative displacements under the horizontal seismic excitation were lower than those under the horizontal–vertical seismic excitation, while the opposite was true for the greater shaking intensity. It is believed that in the latter case, the vertical seismic excitation increased soil densification and ground subsidence, which in turn imposed greater constraints on the station. Chen et al. [22] investigated the effect of the vertical ground motion on the dynamic response characteristics of the central columns in a six-story metro station and the test results revealed that with the increasing ratio of the vertical/horizontal acceleration amplitude, the central columns would undertake much more vertical dynamic axial forces compared to side walls. Che et al. [23] experimentally investigated the dynamic behaviors of a single-story subway station embedded in the dry sand excited by the vertical sinusoidal and vertical random waves, respectively. They found that in both cases there was difference in the acceleration amplitude of the ground between the free-field model and soil-station model. Some attempts were also made to explore the relationship between seismic soil pressures and shear strains of the surrounding ground based on the regression analysis of the experimental data.

Numerical and analytical studies of the effect of RVH on underground tunnels dominate most of the previous work. Extremely limited studies have been dedicated to study the influence of the RVH or incident angle of earthquake waves on the seismic responses of the underground metro station, especially for the experimental studies. In terms of the underground metro station, the existing several experimental studies only focus on the effect of the RVH on certain kinds of structural responses, such as structural relative displacement and dynamic internal force. Experimental studies of the effect of RVH on more comprehensive seismic responses also including the acceleration response and dynamic interaction of soil-station system, dynamic soil normal stress (DSNS) along the side wall of station, and structural dynamic tensile strain (DTS), are not available in the literature. Due to the limited number of the existing experiments, further experimental studies of the seismic behavior of the soil and metro station under different vertical earthquake actions are needed to draw more general conclusion. Therefore, in this study the effect of RVH on the seismic responses of an atrium-style metro station including the acceleration, dynamic soil normal stress DSNS, and DTS are the primary foci. Through series of 1 g shaking table tests, this paper presents the key experimental findings, and an attempt is made to evaluate the effect of the RVH both qualitatively and quantitatively. In addition, this paper also provides insights into the seismic behavior of the atrium-style underground structures, which will help researchers and practitioners to better understand the seismic aspects of these kind of structures to improve their seismic design and construction.

## 2. Shaking Table Tests

### 2.1. Experimental Facility

The series of shaking table tests were conducted using the MTS Company shaking table facility at the State Key Laboratory for Disaster Reduction in Civil Engineering, Tongji University. The shaking table (Figure 1) has six degrees of freedom: two horizontal (X and Y), one vertical (Z), and three rotational, and the main technical parameters are listed in Table 1. The operating frequency range, maximum input accelerations, and maximum loading capacity all satisfy the experimental demands.


**Figure 1.** Photos of the shaking table and flexible-wall container.

**Table 1.** Main technical parameters of the shaking table system.

| Table Size/(m × m) | 4 × 4 |
|---|---|
| Maximum specimen mass/ton | 25 |
| Operating frequency range/Hz | 0.1~50 |
| *X* direction | ±100 |
| Maximum displacement/mm *Y* direction | ±50 |
| *Z* direction | ±50 |
| *X* direction | ±1000 |
| Maximum velocity/(mm/s) *Y* direction | ±600 |
| *Z* direction | ±600 |
| *X* direction | ±4.0 |
| Maximum acceleration (empty table)/g *Y* direction | ±2.0 |
| *Z* direction | ±4.0 |
| *X* direction | ±1.2 |
| Maximum acceleration (with mass 15 ton)/g *Y* direction | ±0.8 |
| *Z* direction | ±0.7 |

A cylindrical flexible-wall container (Figure 1) with diameter 3.0 m and height 1.8 m was adopted. It was made of 5 mm thick rubber membrane. Reinforced bars with a diameter of 4 mm and a spacing of 60 mm were arrayed circumferentially around the exterior of the rubber membrane. The top-ring, base-ring, and four columns were all manufactured from H-shaped steel members. The top-ring was supported by four columns with universal joints, providing the container with full translational and rotational freedom. Furthermore, the rubber membrane was designed to have similar shear stiffness with model soil, in order to minimize any soil-container interactions. The container had been proven to present good lateral shear-type deformations and to be reliable in terms of the negligible influence of the vertical boundary on the specified experiment [24,25].

## 2.2. Model

In view that the similitude ratio placed a severe limitation on the choice of suitable model materials, the similitude ratio design would be conducted before choosing the model materials. Based on the capability of the existing facility and equipment, the similitude ratio design of the experiment was accomplished on the basis of the dimensional analysis, which was adopted extensively in the design of the shaking table tests by other researchers. Meymand [26] designed and performed a series of scale model shaking table testing of the piles in clay in a 1 g scale model environment [27], in which he summarized that the method of the governing equations involved the differential equation describing the process and the formation of the similarity variables that related the model to the prototype. The similitude ratio design for this research herein closely follows the aforementioned method.

With respect to dynamics problems, the differential equation of motion expressed through displacement can be stated as (take the equation of x-direction as an example)

$$(\lambda + G)\frac{\partial \varepsilon}{\partial x} + G\nabla^2 u + X = \rho\frac{\partial^2 u}{\partial t^2} \tag{1}$$

where $u$, $t$, $\rho$, and $\varepsilon$ are displacement, time, density, and strain, respectively. $x$ and $X$ refer to the coordinate position and the force per unit volume in the x direction, respectively. $\lambda$ and $G$ are the Lamé constant and shear modulus, respectively. Hence, Equation (1) is also called the Lamé equation. The problem-solving process of general dynamics problems is reduced to solve the Lamé equation under the given boundary conditions. Then, Equation (1) can be expressed as

$$G = \frac{\rho\frac{\partial^2 u}{\partial t^2} - \lambda\frac{\partial \varepsilon}{\partial x} - X}{\nabla^2 u + \frac{\partial \varepsilon}{\partial x}} \tag{2}$$

The most common sets of basic quantities are those of mass M, length L, and time T [28]. In Equation (2), $\varepsilon$ is a dimensionless quantity and thus the dimension of $\frac{\partial \varepsilon}{\partial x}$ is $L^{-1}$. The dimension of $\rho$ is $ML^{-3}$. The dimension of $\frac{\partial^2 u}{\partial t^2}$, which represents acceleration, a, is $LT^{-2}$. The three items in the numerator have the same dimensions. The two items in the denominator also have the same dimensions. Since $\varepsilon$ is a dimensionless quantity for both prototype and model soil, the similitude ratio for $\varepsilon$ must equal unity (1). The similitude ratios for $\nabla^2 u + \frac{\partial \varepsilon}{\partial x}$ and $\rho\frac{\partial^2 u}{\partial t^2} - \lambda\frac{\partial \varepsilon}{\partial x} - X$ are $S_l^{-1}$ and $S_\rho S_a$, respectively. The similitude ratio for $G$ is $S_{G_d}$, where the subscript $G_d$ represents dynamic shear modulus. Then, the similitude relations between the model soil and the prototype soil can be deduced from Equation (2) as:

$$\frac{G_d^m}{G_d^p} = S_{G_d} = S_\rho S_a S_l \tag{3}$$

where $G_d^m$ and $G_d^p$ are dynamic shear modulus of model and prototype, respectively. $S$ with the subscripts refers to the similitude ratio of the quantities corresponding to those subscripts, i.e., $S_{G_d}$, $S_\rho$, $S_a$, and $S_l$ represent the similitude ratios for soil dynamic shear modulus, soil density, soil acceleration, and soil geometry size, respectively.

The similitude ratios corresponding to other quantities can also be obtained in a similar way. The similitude ratio of the length is set to 1/30 for both the model soil and model station. Table 2 shows the main parameters adopted in defining the similitude relations in this study.

**Table 2.** Similitude relations.

| Types | Properties | Similarity Relations | Similitude Ratios | |
|---|---|---|---|---|
| | | | **Model Structure** | **Model Soil** |
| Geometry | Length $l$ | $S_l$ | 1/30 | 1/30 |
| | Linear displacement $r$ | $S_r = S_l$ | 1/30 | 1/30 |
| Material | Elastic modulus $E$ | $S_E$ | 0.42 | 0.033 |
| | Equivalent density $\rho$ | $S_\rho = S_E S_l^{-1} S_a^{-1}$ | 12.6 | 0.52 |
| | Shear modulus $G$ | $S_G$ | — | 0.033 |
| Dynamic | Mass $m$ | $S_m = S_\rho S_l^3$ | $4.4 \times 10^{-4}$ | $1.2 \times 10^{-6}$ |
| | Acceleration $a$ | $S_a$ | 1 | 1 |
| | Duration $t$ | $S_t = S_E^{-\frac{1}{2}} S_l S_\rho^{\frac{1}{2}}$ | 0.1826 | 0.1826 |
| | Frequency $\omega$ | $S_\omega = 1/S_t$ | 5.48 | 5.48 |
| | Dynamic stress $\sigma$ | $S_\sigma = S_l S_a S_\rho$ | 0.42 | 0.033 |
| | Dynamic strain $\varepsilon$ | $S_\varepsilon$ | 1 | 1 |

To satisfy the aforementioned similitude relations, an artificial model soil made of sand mixed with sawdust was selected, which had been studied and used by other researchers [29]. By targeting the curves of both the shear modulus and damping ratio decaying with the shear strain for the artificial model soil and prototype soil [30], the optimum mass ratio of sawdust to sand was determined to be 1:2.5 through a series of cyclic triaxial tests performed in the laboratory. The comparison of the curves between artificial model soil and prototype soil can be found in [24].

The prototype of the atrium-style metro station had the dimension of 21.3 × 17.7 m (width × height) and had two stories, including the station hall floor and platform floor. No columns on the station hall floor and thin-walled columns with spacing 7.6 m on the platform floor were adopted. Both the ceiling and middle slabs were mostly replaced with the flat-beams, directly resulting in about 50% opening area of the floorage for both slabs. The prototype station was a cast-in-place reinforced concrete structure and the strength grades of concrete and steel rebar were C35 and HRB400, respectively. Galvanized steel wire and micro-concrete were adopted in the model station to represent two practical materials mentioned above. To satisfy the similitude relations, an optimum mass ratio of micro-concrete was determined to be as cement:sand:lime powder:water = 1:5:0.64:1.18 through a series of material tests, and the compressive yield strength and elastic modulus were measured to be 10.68 MPa and $1.32 \times 10^4$ MPa, respectively. Figure 2 shows the details of the model station, including three observation planes. The observation plane-1 was located within the central symmetrical plane of the whole container-soil-structure system, while observation plane-2 and plane-3 were both 50 mm away from it.

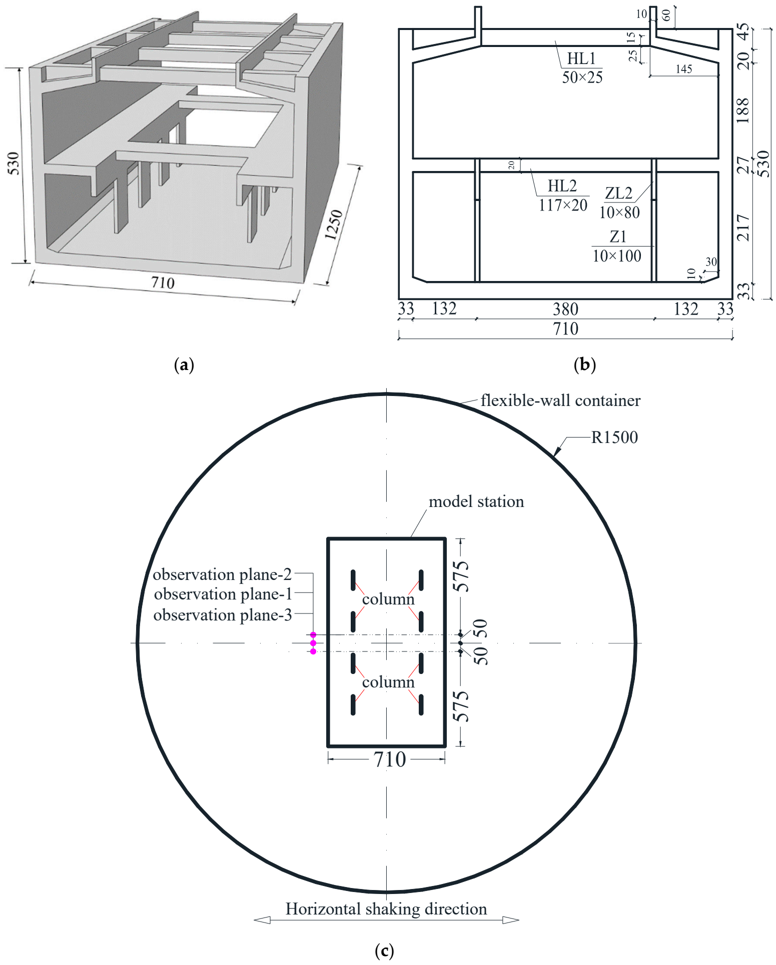


**Figure 2.** Dimensions of the model station: (**a**) perspective view; (**b**) cross-section; (**c**) locations of three observation planes (unit: mm).

For the whole soil-structure system, various real-time data were collected, including the acceleration and displacement in soil and on structure, the dynamic soil normal stress on both the left and right side walls, and the strain produced on the surface of the structural members.

### 2.3. Instrumentation

The locations of these instruments were all based on numerous prior numerical analyses using finite element method [31,32], which are shown in Figure 3.

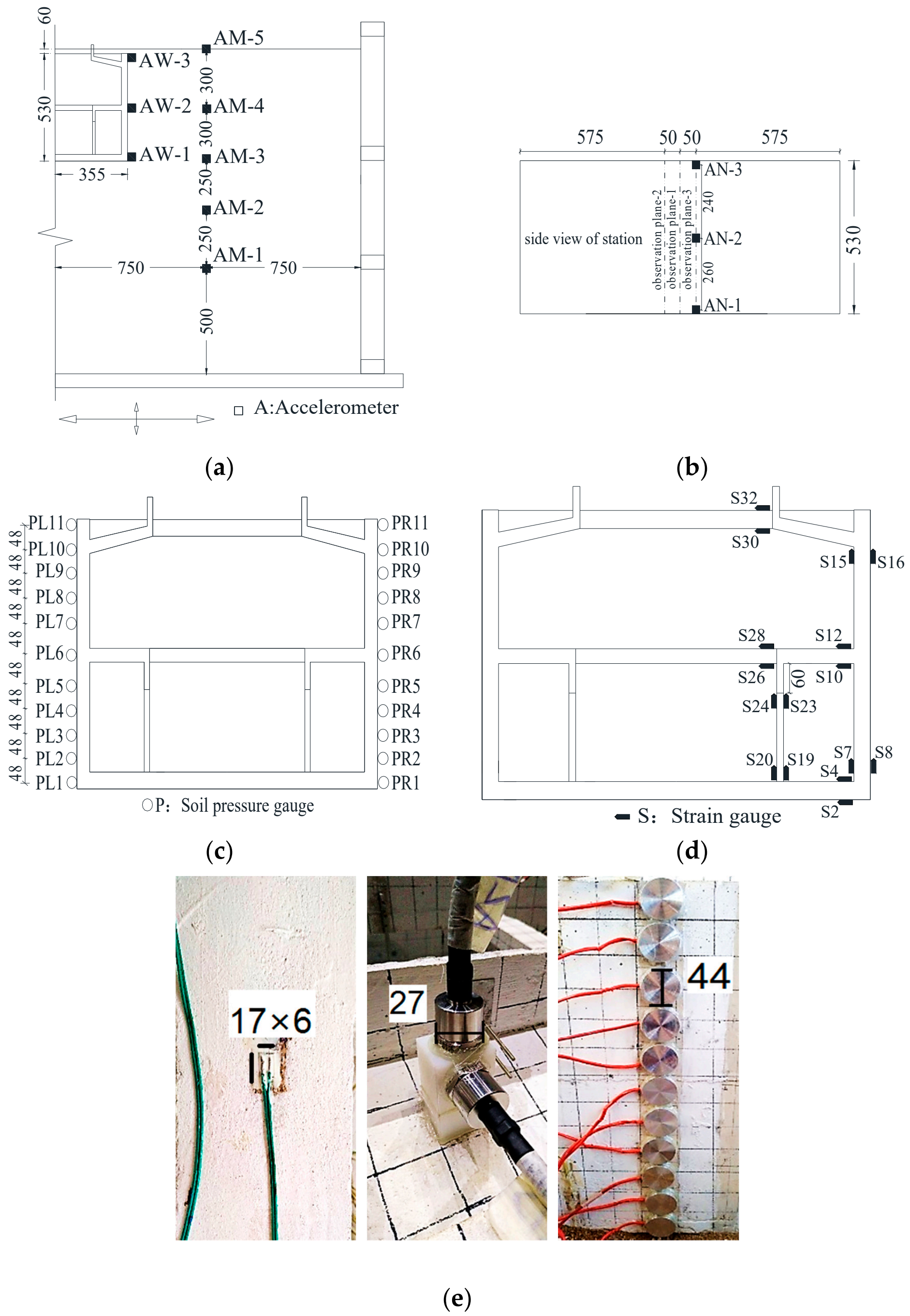


**Figure 3.** Layouts of sensors for soil-station model: (**a**) accelerometers of side wall and soil across the whole depth in observation plane-1; (**b**) accelerometers of soil adjacent to station in observation plane-2; (**c**) soil pressure cells in observation plane-3; (**d**) strain gauges; (**e**) photos of strain gauge, accelerometers, and soil pressure cells (all dimensions in mm).

Five accelerometers (AM-1, AM-2, AM-3, AM-4, and AM-5), as shown in Figure 3a, were placed in the middle between the center of the model soil and the wall of the flexible-wall container to capture the acceleration responses with soil depth. In considering the symmetry, Figure 3a only shows one-half of the whole container-soil-structure system while the accelerometers are completely displayed.

As displayed in Figure 3a,b three accelerometers (AN-1, AN-2, and AN-3) were arrayed in the model soil adjacent to the side wall, which are set to investigate the effects of the underground metro station on the soil acceleration.

Three more accelerometers (AW-1, AW-2, and AW-3) were installed near the previous ones on the side wall to record its acceleration. The depths of the accelerometers AW-1, AW-2, and AW-3 correspond to the depths of the base slab, middle slab, and ceiling slab, respectively. The comparison of the acceleration responses between the two groups of accelerometers is expected to investigate the effect of RVH on the dynamic interaction, which is a most interesting topic for the soil-structure system.

Soil pressure cells PL1–PL11 on the left side wall and PR1–PR11 on the right side wall were arrayed to investigate the amplitude and distribution of the dynamic soil normal stress on the two walls, Figure 3c. The interval between any two adjacent cells was 48 mm, which allowed to capture the essential data and to represent the complex stress distribution along the side wall as stated by the early finite element analyses.

Strain gauges, plotted in Figure 3d, were arrayed to investigate the values and spatial distribution of the structural strain, especially focusing near the joints between different structural components as the ends of the beam, column, side wall, and slab. In Figure 3d the strain gauges S23 and S24 were located on the top of the column (Z1 in Figure 2b), which was just below the longitudinal beam (ZL2 in Figure 2b).

Figure 3e shows the selected photos of various sensors. The experimental procedure is shown in Figure 4.

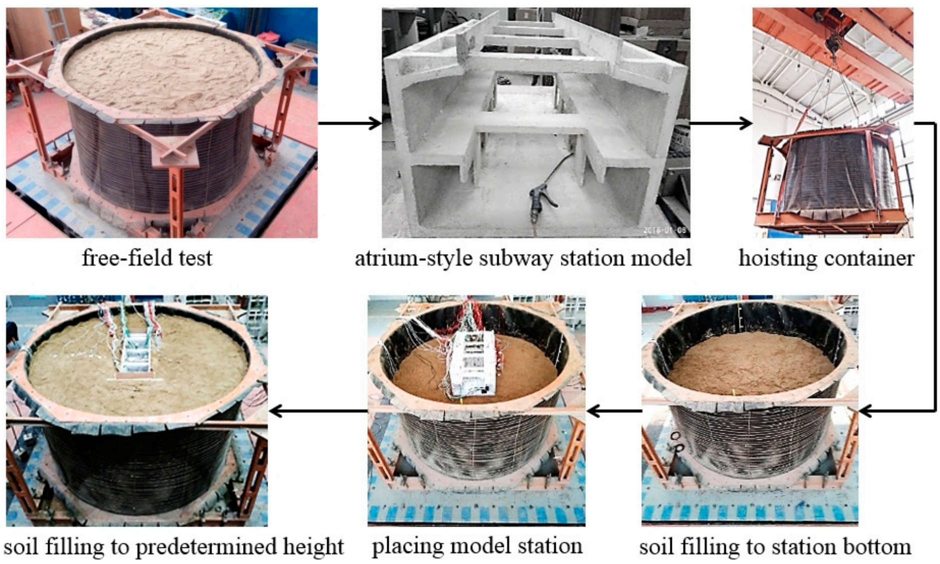


**Figure 4.** Photos of the experimental procedure.

## 2.4. RHV Inputs

The shaking table was accelerated incrementally and the earthquake motion in the horizontal and vertical directions were applied synchronously. The acceleration amplitude of all the horizontal input motions was adjusted to 0.1 g and corresponding vertical acceleration amplitudes were adjusted to 0 g, 0.05 g, 0.1 g, and 0.15 g, respectively. Hence, different RVH that equals to 0, 0.5, 1, and 1.5 are obtained to investigate their influence on the seismic behavior of the soil and buried metro station. For convenience, a strong-motion record of the Loma Prieta, California, earthquake of 18 October 1989 from the PEER

Strong Motion Database [33] was selected as the input motion for both types of the loading mentioned above, whose acceleration time history and corresponding Fourier amplitude spectra, together with target design spectrum of prototype ground concerning the experiment, are shown in Figure 5. It is seen that the acceleration response spectra of the selected 1989 Loma Prieta earthquake matched the target design spectrum well. Table 3 shows the test cases in this study.

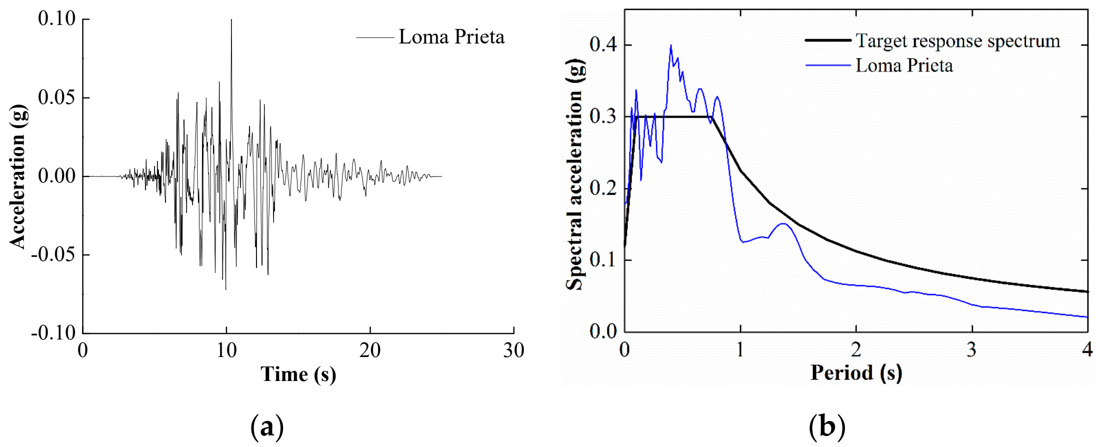


**Figure 5.** The details of Loma Prieta ground motion: (**a**) accelerogram; (**b**) spectral acceleration compared with target design spectrum [34].

**Table 3.** Test cases for the shaking table tests.

| No | Cases | Waveform | Peak Acceleration (g) | |
|---|---|---|---|---|
| | | | Horizontal | Vertical |
| 1 | LP-x0.1 | Loma Prieta | 0.1 | 0 |
| 2 | LP-x0.1-z0.05 | Loma Prieta | 0.1 | 0.05 |
| 3 | LP-x0.1-z0.1 | Loma Prieta | 0.1 | 0.1 |
| 4 | LP-x0.1-z0.15 | Loma Prieta | 0.1 | 0.15 |

The targeted base motions were converted from prototype to model scale units. The base accelerations recorded on the shaking table were refered to as achieved motions. Figure 6 shows the comparison between targeted base motions and achieved base motions both in horizontal and vertical components, including all test cases in Table 3. For any test case, the whole acceleration time history was consistent and minor differences in amplitude were observed between achieved and targeted base motions. These minor differences were acceptable, in view of shaking table performance and such large model specimens.

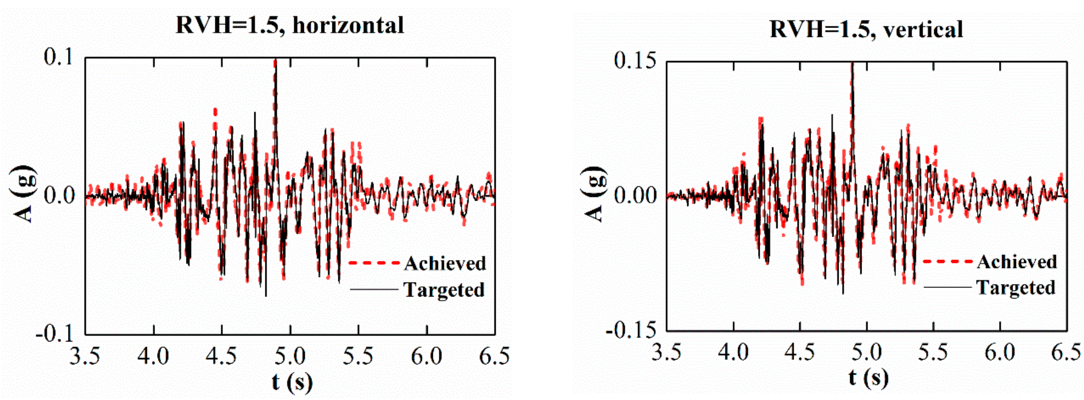


**Figure 6.** *Cont.*

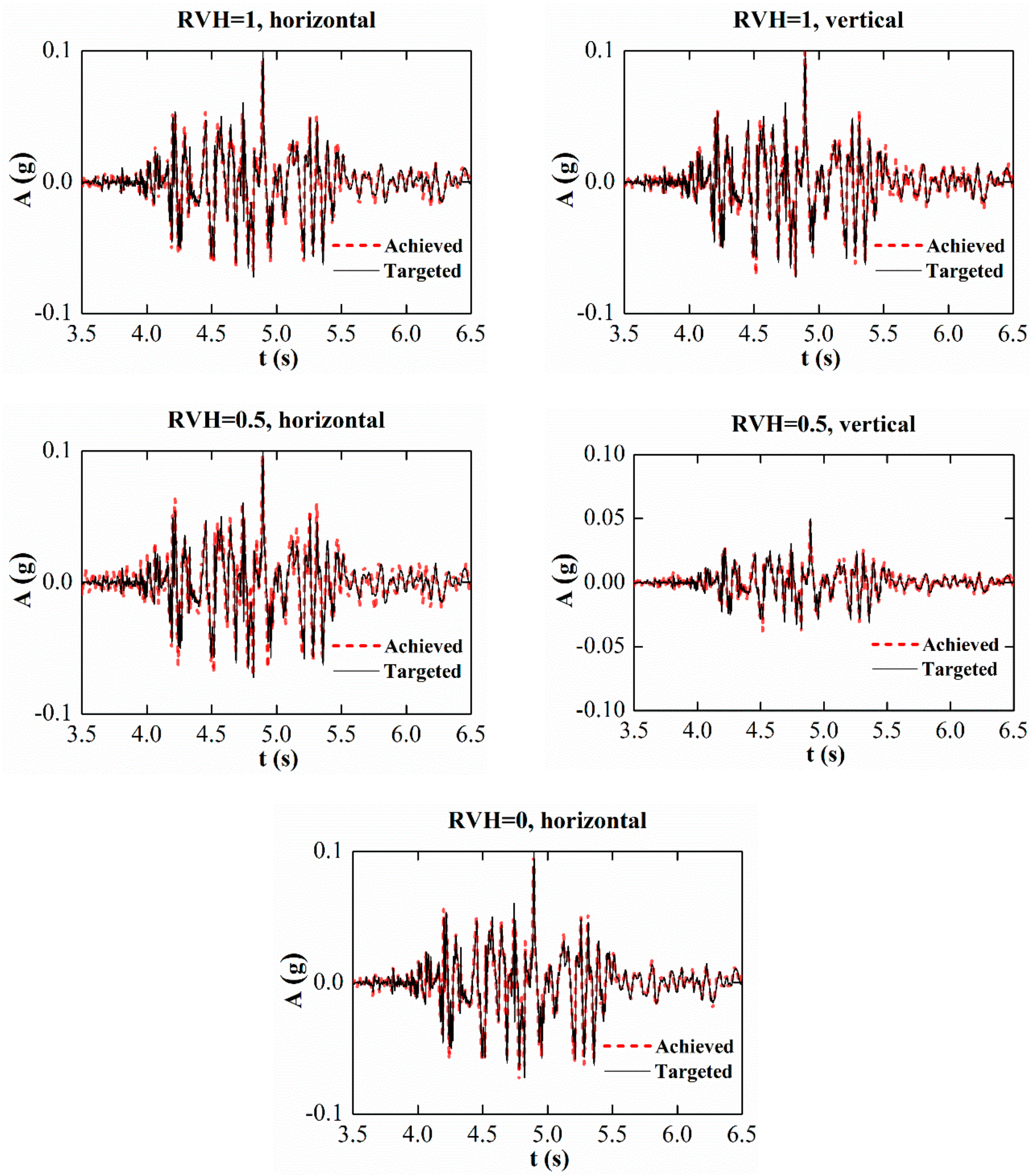


**Figure 6.** Comparison between targeted base motions and achieved base motions both in the horizontal and vertical components for all test cases.

It is worth mentioning that some details of the experimental program, verification of the free-field test, and interpretation of some preliminary results can be found in prior papers [24,25].

## 3. Test Results and Discussion

### *3.1. Influence of RVH on Soil Acceleration*

To investigate the influence of the RVH on the vertical propagation of the waves in the ground, as an example, Figure 7 compares the horizontal acceleration time histories of the soil at different measuring points (AM-1, AM-2, AM-3, AM-4, and AM-5) between RVH = 0 and RVH = 1. It is seen that at any measuring point their horizontal acceleration always behaves consistently in the trend, and the differences mainly lie in the amplitude. For both RVH = 0 and RVH = 1, the horizontal acceleration of the soil increases with decreasing depth.

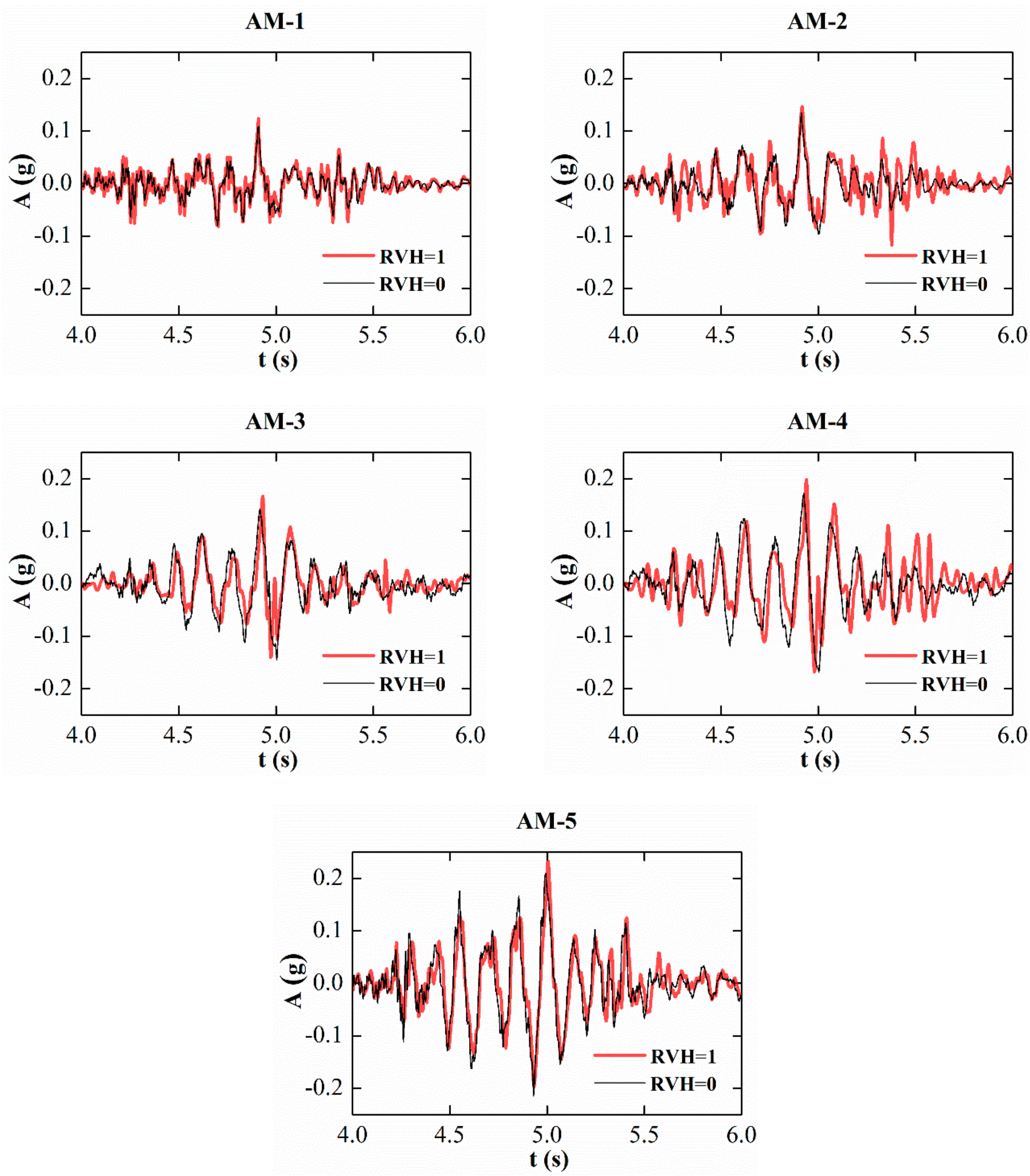


**Figure 7.** Comparison of horizontal acceleration time histories of soil between RVH = 0 and RVH = 1. RVH: ratio of vertical to horizontal peak ground acceleration.

To better evaluate the trend of the horizontal acceleration amplitude, the acceleration amplification factor (AAF) is obtained by dividing the peak horizontal acceleration at each measuring point by the peak horizontal acceleration of input motion. Therefore, the AAF at the base of the model (at soil depth of 1.6 m in Figure 3a) is equal to unity (1). This definition also applies to the following parts. Figure 8 shows the AAF of the ground along the depth under different RVH. The horizontal acceleration amplitude of the soil tends to increase from the bottom to the ground surface. Under the four conditions the AAFs on the ground surface are about 2.3–3.1 and the soil presents significant amplification. This is reasonable since the amplitude of all the input motions are relatively low.

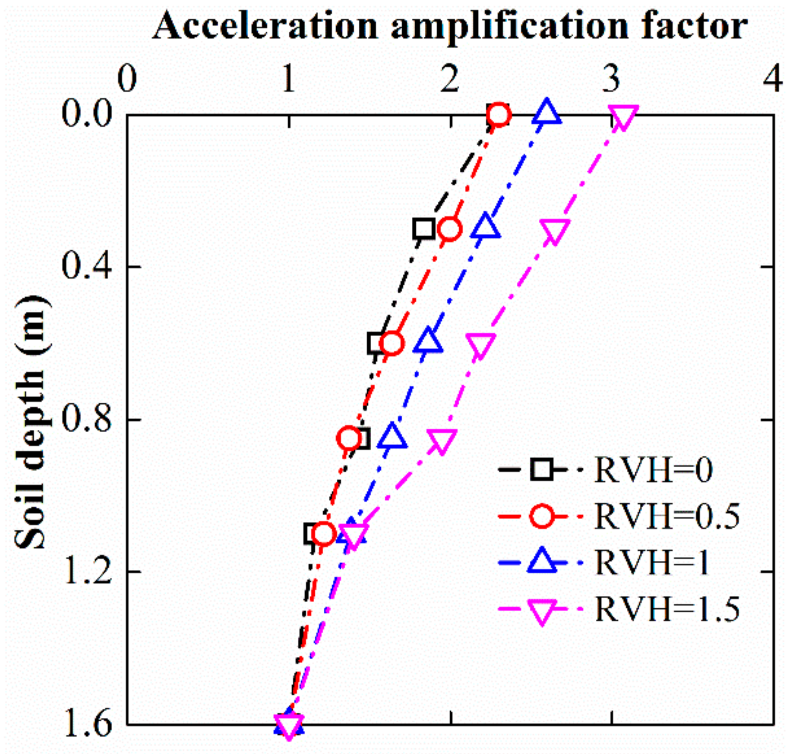


**Figure 8.** Acceleration amplification factor of ground under different RVH.

In terms of the acceleration levels in this study, with increasing RVH, soil horizontal acceleration increases and the increase in the amplitude grows significantly with increasing RVH on the whole. It demonstrates that soil horizontal acceleration is more sensitive to higher RVH or higher vertical acceleration.

*3.2. Acceleration Difference between the Side Wall and Adjacent Soil*

To investigate the influence of the RVH on the acceleration response difference between the side wall and adjacent soil, Figure 9 illustrates the comparison of the acceleration time histories between side wall and adjacent soil at three different depths, which are ceiling slab (Figure 9a), middle slab (Figure 9b), and base slab (Figure 9c), respectively.

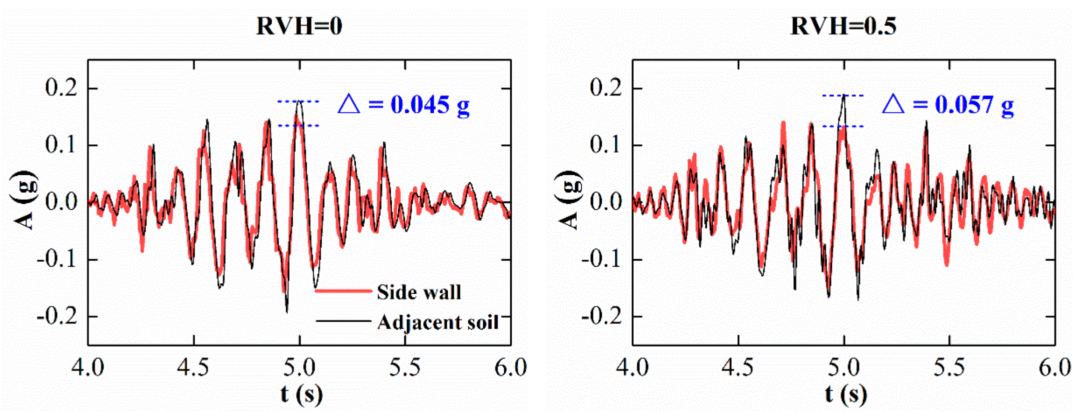


**Figure 9.** *Cont.*

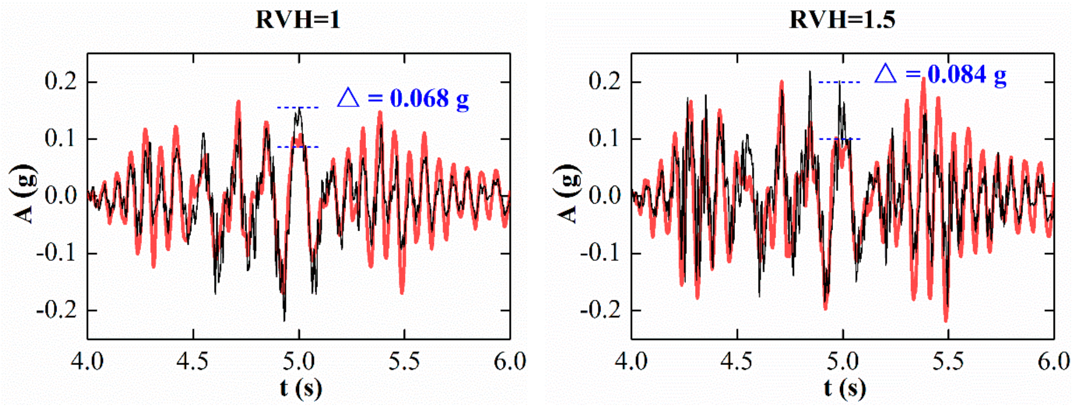


(a)

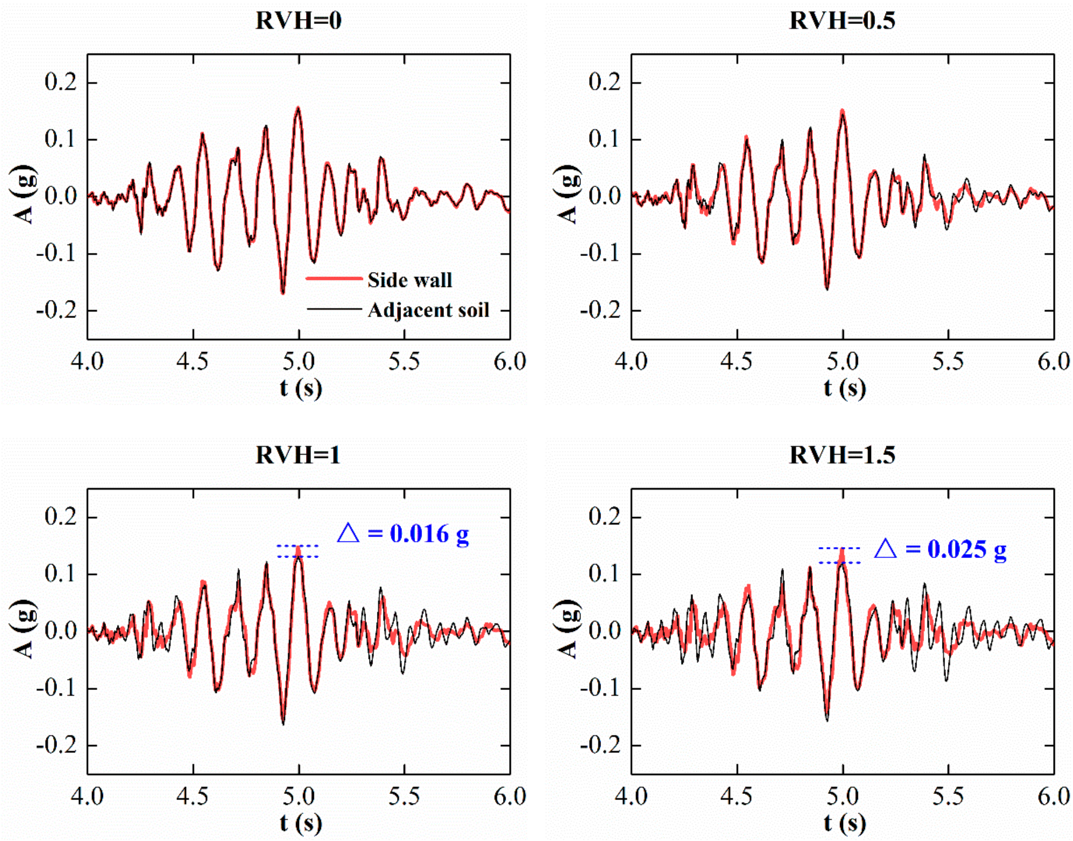


(b)

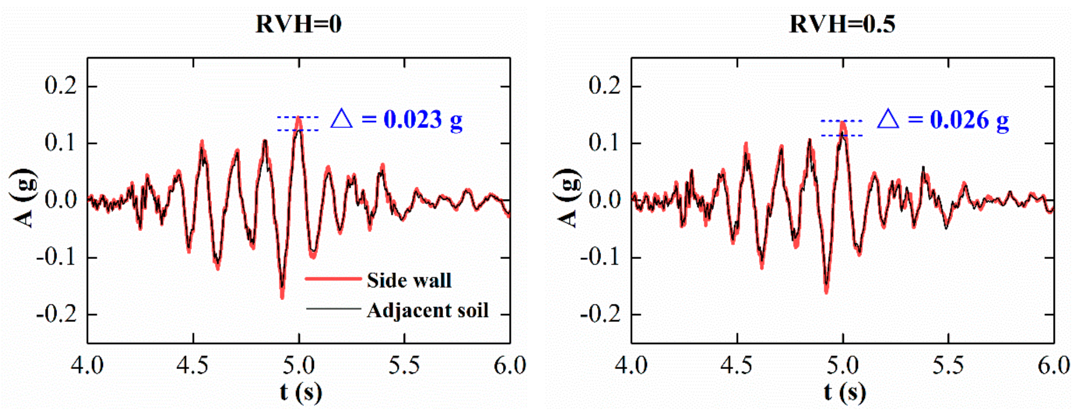


**Figure 9.** *Cont.*

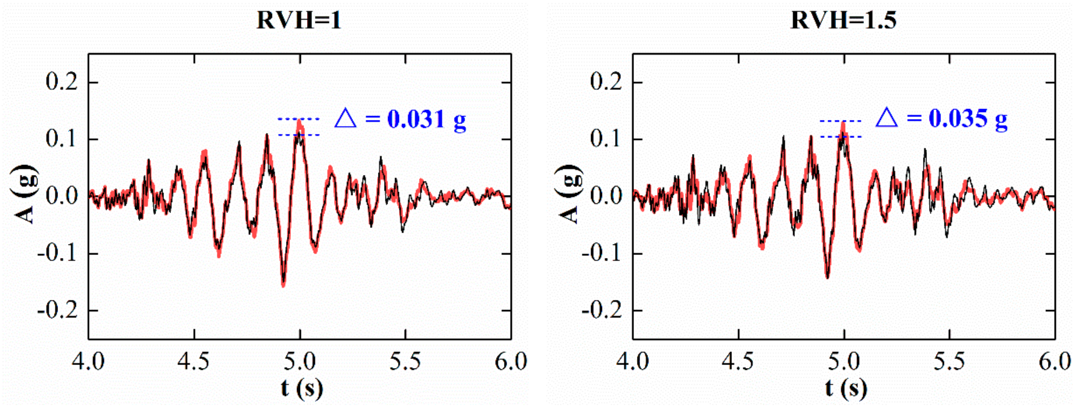


(**c**)

**Figure 9.** Comparison of the acceleration time histories between side wall and adjacent soil. at three different depths: (**a**) comparison at depth of ceiling slab; (**b**) comparison at depth of middle slab; (**c**) comparison at depth of base slab.

As can be seen from Figure 9, the phases of the side wall and adjacent soil are always consistent at three depths. The acceleration difference between the side wall and the adjacent soil mainly lies on the amplitude. For the side wall and the adjacent soil, the amplitude of them is almost the same at the depth of the middle slab, where the amplitude differences are about 0–0.025 g at the peak-strain moment. The amplitude of them has minor differences at depth of base slab, where the amplitude differences are about 0.023–0.035 g at the peak-strain moment. It is worth mentioning that some larger differences between the side wall and adjacent soil can be observed at the depth of the ceiling slab, where the amplitude differences reach about 0.045–0.084 g at the peak-strain moment. Under RVH = 1.5 and horizontal input acceleration of 0.1 g, the aforementioned amplitude difference even reaches 0.084 g. It reveals larger differences in the horizontal acceleration between the side wall and the adjacent soil at the depth of the ceiling slab. The differences can be attributed to that the ceiling slab lies too close to the ground surface and there is a significant amplification of the acceleration responses since fewer soil constraints exist there. It reveals that for the underground structures with zero or near-zero buried depth, such as atrium-style metro stations, special attention should be paid to the acceleration response difference between the structure and adjacent soil.

In order to investigate the differences of the horizontal acceleration amplitude between the side wall and the adjacent soil with increasing RVH, the results at three different depths are depicted in Figure 10. It is found that at any depth, the acceleration differences between side wall and adjacent soil appear a linear increase in the amplitude as RVH increases from 0 to 1.5. With regard to the amplitude, the acceleration differences at the depth of the ceiling slab are larger than those at the depth of the base slab. The acceleration differences at the depth of the middle slab are the smallest ones among the three depths. With regard to the increasing rates, the increasing rate at the depth of the ceiling slab is about 2.56%, which is larger than that of 1.65% at the depth of the middle slab. The smallest one is 0.82% at the depth of the base slab.

In conclusion, for an atrium-style metro station, the differences in the horizontal acceleration amplitude between the structure and the adjacent soil rise with increasing RVH, which are different at different depths. The most significant differences occur at the depth of the ceiling slab. The RVH has a significant influence on the dynamic soil-structure interaction, especially for higher RVH.

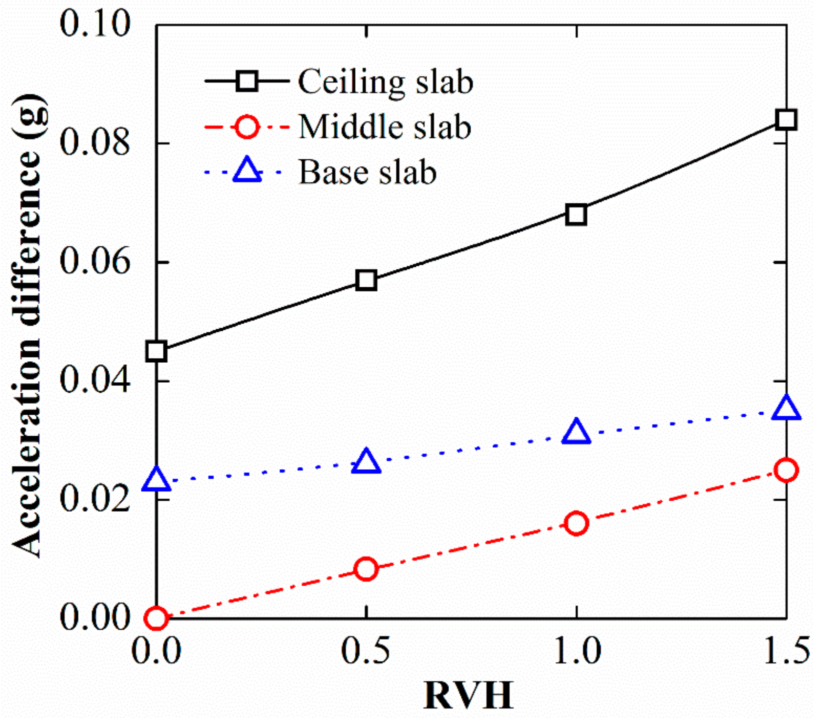


**Figure 10.** The difference of horizontal acceleration amplitude with increasing RVH between side wall and adjacent soil at three different depths.

### 3.3. *Influence of RVH on Dynamic Soil Normal Stress*

Dynamic soil normal stress (DSNS) is defined as the difference between the total stress and initial static stress along the side wall of the model station. As an example, Figure 11 compares the two time histories of the DSNS between RVH = 0 and RVH = 1. It is found that the time histories of the DSNS resemble that of the input motion. The essence of this phenomenon is also revealed by Kramer, who points out that the input seismic excitation in the form of an acceleration can be converted into a stress wave [35]. With different RVH their phases are basically consistent at all measuring points, though the amplitudes of the DSNS behave differently at different depths of the side wall. For example, the amplitudes are almost the same near the bottom of the side wall (e.g., PR1 and PR2) while the amplitudes under RVH = 1 are always larger than those under RVH = 0 at other depths of the side wall (e.g., PR3~PR11).

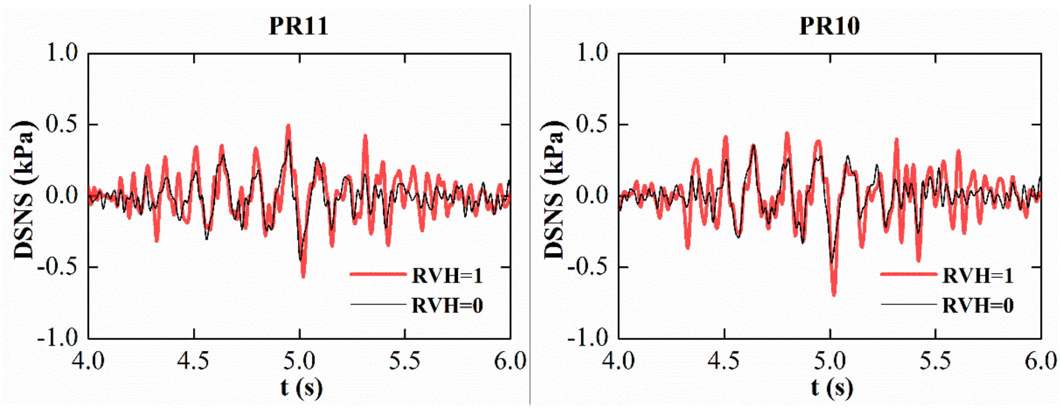


**Figure 11.** *Cont.*

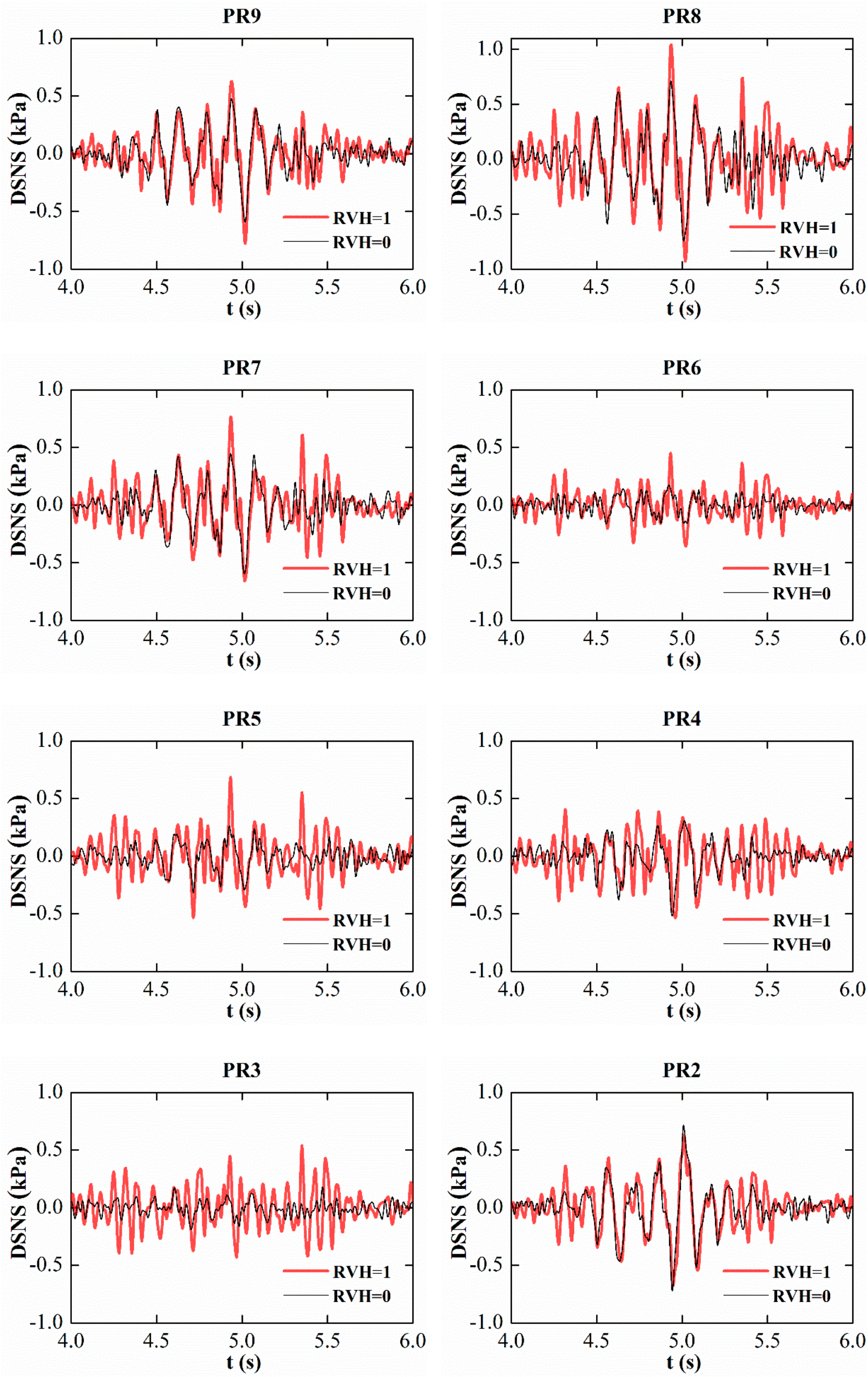


**Figure 11.** *Cont.*

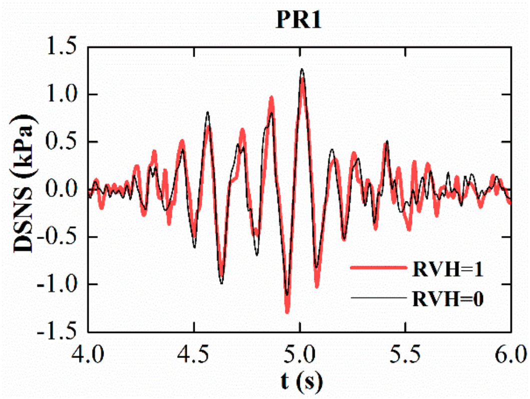


**Figure 11.** Comparison of time histories of dynamic soil normal stress (DSNS) along right side wall between RVH = 0 and RVH = 1.

To figure out the influence of the RVH on the DSNS along the side wall, Figure 12 displays the peak DSNS along the left and right side walls under different RVH.

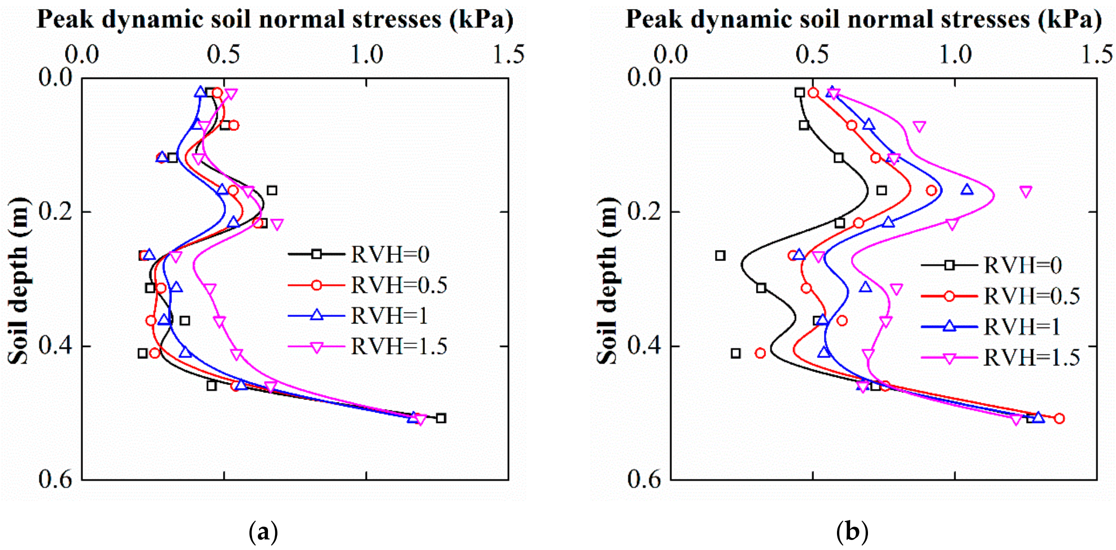


**Figure 12.** Distribution of peak DSNS under different RVH along (**a**) left side wall, and (**b**) right side wall.

As can be seen from Figure 12a, under the input motion of Loma Prieta, peak DSNS along the left side wall follows an approximate L–shaped distribution. With increasing RVH, on the whole, there is no significant change in the amplitude of the peak DSNS. Compared to other RVH, a relatively large increase at the depth of the platform floor can be observed when RVH equals to 1.5.

With respect to the peak DSNS along the right wall, as shown in Figure 12b, at the depth between the top of the right side wall and the middle of the station hall floor, they all follow an approximately linear distribution. At the depth between the middle of the station hall floor and the bottom of the right side wall, they all follow an approximately ∑–shaped distribution. It is worth mentioning that the maximum stress occurs at the bottom of the side wall basically. With increasing RVH, peak DSNS along the right wall increase on the whole, except for the bottom of the side wall (base slab level). Compared to the results under only horizontal input motion (RVH = 0), the maximum increase in peak DSNS under RVH = 0.5, 1, and 1.5 reach about 148%, 159%, and 199%, respectively. For the bottom of the side wall (base slab level), with increasing RVH, the peak DSNS has no significant change, which is different from the situation at other position of the side wall and has also been concluded above from Figure 11. It might be attributed to the sharp transition in the corner and a possible stress concentration there.

When comparing the distribution of the peak DSNS between the left and right side walls, some obvious differences between them can be found. A similar finding was also drawn from a numerical study of a shallow buried rectangular underground structure under earthquake loading with both the horizontal and vertical components [36]. The differences in stress distribution of the peak DSNS between the left and right side walls can be explained by the shadow effect, which is caused by the entrapment of the waves between the ground and the underground structure [37]. With increasing RVH, the above-mentioned differences between the left and right side walls also increase. From the perspective of dynamic soil normal stress, the experimental results have proven that RVH has significant influence on the dynamic soil-structure interaction.

### 3.4. Influence of RVH on Structural Dynamic Strain

The dynamic strain is defined as the difference between the total strain during shaking and initial static strain before shaking. As an example, Figure 13 compares the time histories of the dynamic strain between RVH = 0 and RVH = 1 from one side of every cross section (Figure 3d). Just as the characteristics of the DSNS mentioned earlier, the time histories of the dynamic strain also resemble that of the input motion. In terms of the two different RVH, their phases are extremely consistent for all the measuring points and their amplitudes have minor differences for most of the measuring points.

Figure 14 shows the variation of the peak dynamic tensile strain (DTS) with different RVH for different measuring points of the model station. To easily observe the rate of change in the dynamic strain over different RVH, the value of the y–coordinate in Figure 14 represents the ratio of the peak DTS under RVH = i (i = 0, 0.5, 1, and 1.5) to that under RVH = 0. Since two strain gauges are arranged for every cross section (Figure 3d), the strain results on one side are displayed in Figure 14a and the opposite ones are shown in Figure 14b, where the layouts of corresponding strain gauges are plotted again. As can be seen from Figure 14a, with increasing RVH, the DTS will change in an undulating fashion (decrease, increase, and decrease again), which is different from the response characteristics of the soil, in that the soil acceleration at any depth increases rapidly with increasing RVH. It means the influence of the RVH on the structural DTS is rather complex.

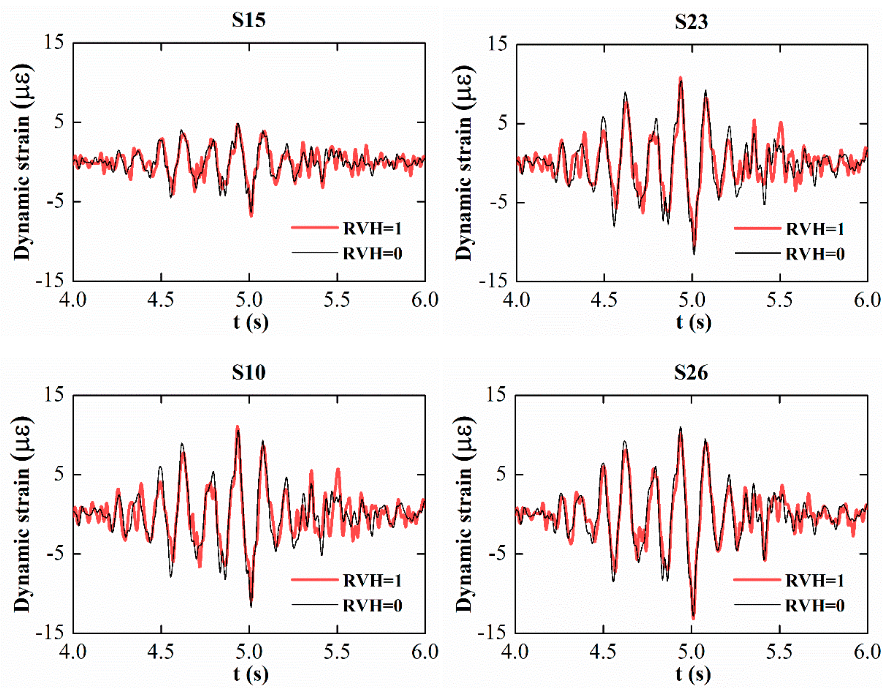


**Figure 13.** *Cont.*

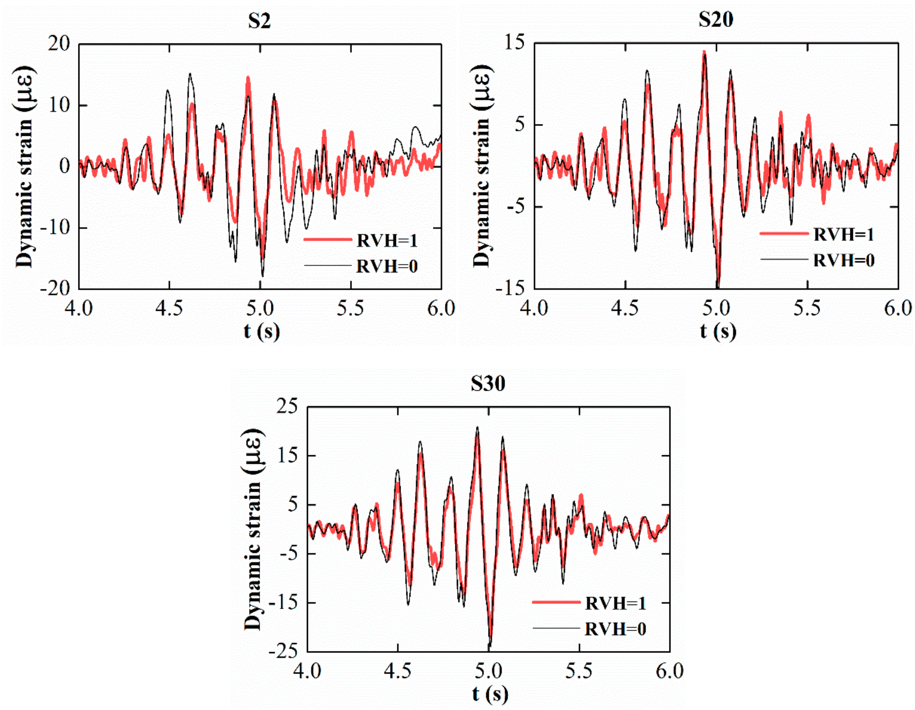


**Figure 13.** Comparison of time histories of dynamic strain on one side of structural components between RVH = 0 and RVH = 1.

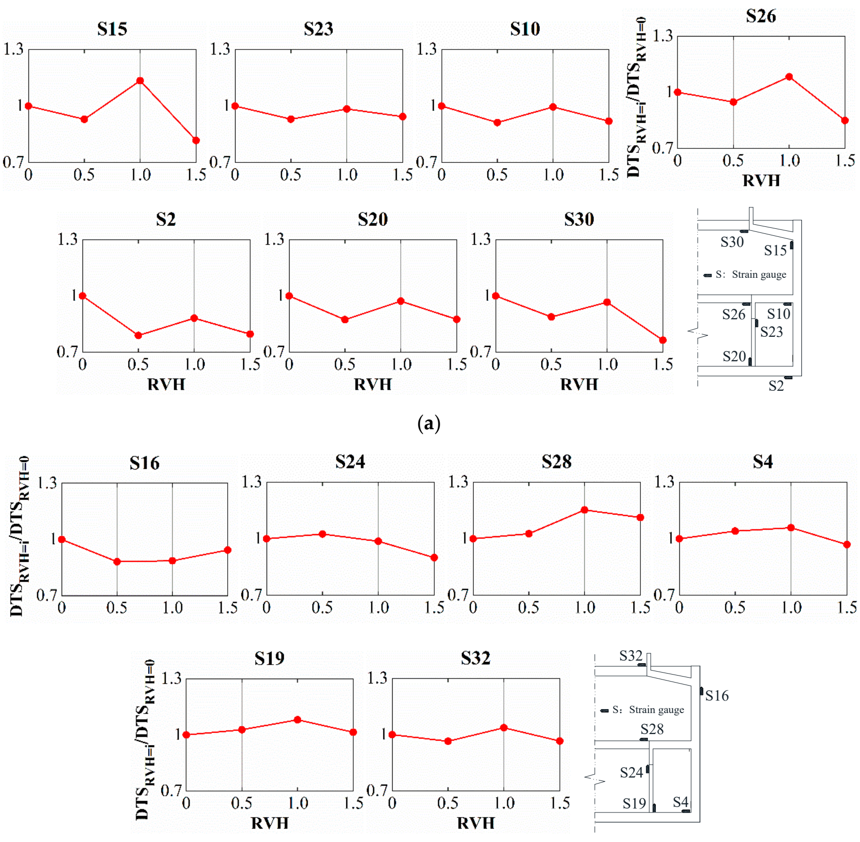


**Figure 14.** Peak dynamic tensile strain (DTS) of model station under different RVH: (**a**) strains on one side; and (**b**) strains on another side.

The soil and structure behave differently in the seismic responses with increasing RVH. It can also be seen from Figure 14a that the DTS with bidirectional input motion may be less than those with only horizontal input motion (the value of the y–coordinate is less than 1). This conclusion is verified by the numerical simulation conducted on a prototype atrium-style metro station [31], and can also be found in [38]. This phenomenon can be explained as follows: the presence of a cavity can cause, under certain conditions, intense and selective de-amplification of the free-filed motion, which is referred to as "shadow zone" [37]. When comparing the results of the DTS in Figure 14a,b, for every cross section, the DTS on one side is not equal to the opposite one. It reveals that the stresses in the cross section of every structural element are uneven under bidirectional input motion.

## 4. Conclusions

An atrium-style metro station is a favorite choice owing to its excellence in providing a larger and clearer space for the passengers and commercial clients at the station hall floor. However, concern for the seismic safety of such a station is growing since its hall slabs are replaced with the flat-beams. Tests are needed for the evaluation of its seismic safety. A series of 1 g shaking table tests were conducted to investigate the seismic responses of an atrium-style metro station.

In this study, extensive experimental results were presented to investigate the influence of the RVH (ratio of vertical to horizontal peak ground acceleration) on the seismic responses of both the soil and the underground metro station. Results show that the acceleration amplification factors (AAFs) on the ground surface are about 2.3–3.1, and that the soil presents significant amplification under several considered conditions. Soil horizontal acceleration is more sensitive to the higher RVH or higher vertical acceleration. Significant differences in horizontal acceleration amplitude between the side wall and the adjacent soil at the depth of the ceiling slab are found, and attention should be paid to these kind of differences for the underground structures with zero or near-zero buried depth, such as atrium-style metro stations. With increasing RVH, the differences in the horizontal acceleration amplitude between the side wall and the adjacent soil also rise. The RVH has a significant influence on the dynamic interaction, especially for higher RVH. Under the input motion of Loma Prieta, the distribution of the peak DSNS (dynamic soil normal stress) along the left and right side walls represents significant difference. The peak DSNS along the left side wall follows an approximate L-shaped distribution, while it is different for the right side wall. With increasing RVH, there is no significant change in the amplitude of the peak DSNS along the left side wall on the whole, while it increases a lot (the maximum increase reach about 148%, 159%, and 199% under RVH = 0.5, 1, and 1.5 when comparing with that under RVH = 0) for the right side wall. The soil and structure behave differently in the seismic responses with increasing RVH. The stresses in the cross-section of every structural element are uneven under horizontal–vertical earthquake excitation.

In conclusion, from the perspective of the soil acceleration, structural acceleration, and dynamic soil normal stresses along the side wall of station, experimental results have proven that ratio of vertical to horizontal peak ground acceleration (RVH) has significant influence on the dynamic soil-structure interaction. It is believed that under extreme earthquake loading, such as near fault zones, RVH is a parameter of paramount importance and should be accounted for in the seismic analyses and seismic performance assessments of the underground structures, especially for those with zero or near-zero buried depth, such as atrium-style metro stations.

It is worth mentioning that further investigation of the effect of the vertical earthquake motion is essential through a series of numerical analyses using a minimum number of the earthquake records specified by a certain code. In this way, a cross-check of the findings from the multiple records could be expected to accomplished and this is a work in progress.

**Author Contributions:** Test scheme, Z.Z., Y.Y., H.Z., and H.Y.; experimental works, Z.Z.; discussion and analysis, E.B. and Y.Y.; writing—original draft preparation, Z.Z.; writing—review and editing, E.B. and Y.Y.; funding acquisition, Y.Y. and H.Z.

**Funding:** This research was funded by the National Key Research and Development Plan of China (Grants Nos. 2018YFC1504305, 2018YFC0809600, 2018YFC0809602, and 2017YFC1500703), the State Key Laboratory of Disaster Reduction in Civil Engineering, Tongji University (Grant No. SLDRCE15-02), and the China Scholarship Council (Grant No. 201706260143).

**Conflicts of Interest:** The authors declare no conflict of interest.

## References

1. Papazoglou, A.J.; Elnashai, A.S. Analytical and field evidence of the damaging effect of vertical earthquake ground motion. *Earthq. Eng. Struct. Dyn.* **1996**, *25*, 1109–1137. [CrossRef]
2. Building Research Institute. *Final Report of Damage Survey of the 1995 Hyogoken-Nanbu Earthquake*; Building Research Institute: Tsukuba, Japan, 1996.
3. Goltz, J. *The Northridge, California Earthquake of January 17, 1994: General Reconnaissance Report*; Report No. NCEER-94-0005; University at Buffalo: Buffalo, NY, USA; National Centre for Earthquake Engineering Research: Buffalo, NY, USA, 1994.
4. Mitchell, D.; Tinawi, R.; Sexsmith, R.G. Performance of bridges in the 1989 Loma Prieta earthquake—lessons for Canadian designers. *Can. J. Civ. Eng.* **1991**, *18*, 711–734. [CrossRef]
5. Liang, T.C.; Lin, Y.L. Ground vibrations detection with fiber optic sensor. *Opt. Commun.* **2012**, *285*, 2363–2367. [CrossRef]
6. Nedoma, J.; Stolarik, M.; Fajkus, M.; Pinka, M.; Hejduk, S. Use of fiber-optic sensors for the detection of the rail vehicles and monitoring of the rock mass dynamic response due to railway rolling stock for the civil engineering needs. *Appl. Sci.* **2019**, *9*, 134. [CrossRef]
7. Uenishi, K.; Sakurai, S. Characteristic of the vertical seismic waves associated with the 1995 Hyogo-ken Nanbu (Kobe), Japan earthquake estimated from the failure of the Daikai Underground Station. *Earthq. Eng. Struct. Dyn.* **2000**, *29*, 813–821. [CrossRef]
8. An, X.; Shawky, A.A.; Maekawa, K. The collapse mechanism of a subway station during the Great Hanshin earthquake. *Cem. Concr. Compos.* **1997**, *19*, 241–257. [CrossRef]
9. Moore, I.D.; Guan, F. Three-dimensional dynamic response of lined tunnels due to incident seismic waves. *Earthq. Eng. Struct. Dyn.* **1996**, *25*, 357–369. [CrossRef]
10. Stamos, A.A.; Beskos, D.E. Dynamic analysis of large 3-D underground structures by the bem. *Earthq. Eng. Struct. Dyn.* **1995**, *24*, 917–934. [CrossRef]
11. Stamos, A.A.; Beskos, D.E. 3-D seismic response analysis of long lined tunnels in half-space. *Soil Dyn. Earthq. Eng.* **1996**, *15*, 111–118. [CrossRef]
12. Lee, V.W.; Trifunac, M.D. Response of tunnels to incident SH-waves. *J. Eng. Mech. Div. ASCE* **1979**, *105*, 643–659.
13. Lee, V.W.; Manoogian, M.E. Surface motion above an arbitrary shape underground cavity for incident SH waves. *Eur. Earthq. Eng.* **1995**, *1*, 3–11.
14. Manoogian, M.E.; Lee, V.W. Diffraction of SH-Waves by subsurface inclusions of arbitrary shape. *J. Eng. Mech.* **2002**, *122*, 123–129. [CrossRef]
15. Wong, K.C.; Datta, S.K.; Shah, A.H. Three-dimensional motion of buried pipeline. I: Analysis. *J. Eng. Mech.* **1986**, *112*, 1319–1337. [CrossRef]
16. Huang, J.; Du, X.; Zhao, M.; Zhao, X. Impact of incident angles of earthquake shear (S) waves on 3-D non-linear seismic responses of long lined tunnels. *Eng. Geol.* **2017**, *222*, 168–185. [CrossRef]
17. Sun, C.; Wang, Q. Dynamic response of underground structure under vertical earthquake action. *Appl. Mech. Mater.* **2011**, *105–107*, 1480–1483. [CrossRef]
18. Xu, H.; Li, T.; Xia, L.; Zhao, J.X.; Wang, D. Shaking table tests on seismic measures of a model mountain tunnel. *Tunn. Undergr. Sp. Technol.* **2016**, *60*, 197–209. [CrossRef]
19. Wang, F.; Jiang, X.; Niu, J. The large-scale shaking table model test of the shallow-bias tunnel with a small clear distance. *Geotech. Geol. Eng.* **2017**, *35*, 1093–1110. [CrossRef]
20. Zhao, X.; Shuping, J.; Yi, Y. Study on shaking table model test scheme of tunnel subjected to near-fault pulse-like ground motions. *Mod. Appl. Sci.* **2014**, *8*, 126–139. [CrossRef]
21. Zhao, D.; Gong, B.; Yan, C. Experimental analysis of vibration behavior for large-span underground structure. *J. Civ. Archit. Environ. Eng.* **2002**, *24*, 52–57.

22. Chen, W. Static Pushover and Dynamic Response Characteristics of a Multi-Story Subway Station under Near-Fault Ground Motions. Master's Thesis, Tongji University, Shanghai, China, 2016; pp. 64–69.
23. Che, A.L.; Iwatate, T.; Ge, X.R. Dynamic behaviors of subway structure subjected to strong earthquake motions using shaking table tests and dynamic analyses. *Yantu Lixue/Rock Soil Mech.* **2006**, *27*, 1293–1298. [CrossRef]
24. Zhang, Z.; Yuan, Y.; Bilotta, E.; Yu, H.; Zhao, H. Design of shaking table tests on atrium-style subway station models under seismic excitations. In *Tunnels and Underground Cities: Engineering and Innovation Meet Archaeology, Architecture and Art, Proceedings of the World Tunnel Congress, Naples, Italy, 3–9 May 2019*; Peila, D., Viggiani, G., Celestino, T., Eds.; CRC Press: Leiden, The Netherlands, 2019; Paper No. 92982; pp. 1242–1251. [CrossRef]
25. Zhang, Z.; Bilotta, E.; Yuan, Y.; Zhao, H.; Yu, H. Experimental study on seismic ground motion amplification pattern of soil-structure interaction system. In Proceedings of the 7th International Conference on Earthquake Geotechnical Engineering, Rome, Italy, 17–20 June 2019. Paper No. 11063.
26. Meymand, P.J. Shaking Table Scale Model Tests of Nonlinear Soil-Pile-Superstructure Interaction in Soft Clay. Ph.D. Thesis, University of California, Berkeley, CA, USA, 1998.
27. Moss, R.E.S.; Crosariol, V.A. Scale Model shake table testing of an underground tunnel cross section in soft clay. *Earthq. Spectra* **2013**, *29*, 1413–1440. [CrossRef]
28. Moncarz, P.D.; Krawinkler, H. *Theory and Application of Experimental Model. Analysis in Earthquake Engineering*; John A. Blume Earthquake Engineering Center, Stanford University: Stanford, CA, USA, 1981.
29. Chen, Z.; Chen, W.; Li, Y.; Yuan, Y. Shaking table test of a multi-story subway station under pulse-like ground motions. *Soil Dyn. Earthq. Eng.* **2016**, *82*, 111–122. [CrossRef]
30. Bao, Z.; Yuan, Y.; Yu, H. Multi-scale physical model of shield tunnels applied in shaking table test. *Soil Dyn. Earthq. Eng.* **2017**, *100*, 465–479. [CrossRef]
31. Zhang, Z.; Yu, H.; Yuan, Y.; Zhao, H. 3D numerical simulation of seismic characteristics of atrium-style metro station. In Proceedings of the 3rd International Conference on Performance Based Design in Earthquake Geotechnical Engineering, Vancouver, BC, Canada, 16–19 July 2017. Paper No. 145.
32. Zhang, Z.; Yuan, Y.; Bilotta, E.; Yu, H.; Zhao, H. Dynamic soil normal stresses on side wall of a subway station. In *Life Cycle Analysis and Assessment in Civil Engineering: Towards an Integrated Vision, Proceedings of the Sixth International Symposium on Life-Cycle Civil Engineering, Ghent, Belgium, 28–31 October 2018*; Caspeele, R., Taerwe, L., Frangopol, D.M., Eds.; CRC Press: Leiden, The Netherlands, 2018; Paper No. 345; p. 284. [CrossRef]
33. Pacific Earthquake Engineering Research Center (PEER). *User's Manual for the Peer Ground Motions Data Base Web Application*; The Peer Center, University of California: Berkeley, CA, USA, 2010; Available online: https://ngawest2.berkeley.edu (accessed on 27 January 2018).
34. National Standard of the People's Republic of China. *Code for Seismic Design of Buildings (GB 50011–2010)*; China Architecture & Building Press: Beijing, China, 2010; pp. 33–35.
35. Kramer, S.L. *Geotechnical Earthquake Engineering*; Prentice Hall: Upper Saddle River, NJ, USA, 1996.
36. Xu, Z.; Du, X.; Xu, C.; Hao, H.; Bi, K.; Jiang, J. Numerical research on seismic response characteristics of shallow buried rectangular underground structure. *Soil Dyn. Earthq. Eng.* **2019**, *116*, 242–252. [CrossRef]
37. Yiouta-Mitra, P.; Kouretzis, G.; Bouckovalas, G.; Sofianos, A. Effect of underground structures in earthquake resistant design of surface structures. *Geotech. Spec. Publ.* **2007**. [CrossRef]
38. Mwafy, A.; Elnashai, A. Vulnerability of code-compliant RC buildings under multi-axial earthquake loading. In Proceedings of the 4th International Conference on Earthquake Engineering, Taipei, Taiwan, 12–13 October 2006.